J. Chem. Sci. (2020)132:19
https://doi.org/10.1007/s12039-019-1726-2

REGULAR ARTICLE

Quantitative investigation on the intermolecular interactions present in 8-(4-ethoxyphenyl)-1,3-dimethyl-3,7-dihydro-1H-purine-2,6-dione with insight from interaction energies, energy framework, electrostatic potential map and fingerprint analysis

RAHUL SHUKLA[a], PRABAL BANDOPADHYAY[b], MANISHA SATHE[b] and DEEPAK CHOPRA[a,*]

[a]Crystallography and Crystal Chemistry Laboratory, Department of Chemistry, Indian Institute of Science Education and Research Bhopal, Bhopal By-Pass Road, Bhopal 462 066, Madhya Pradesh, India
[b]Defence Research and Development Establishment (DRDE), Gwalior 474 002, Madhya Pradesh, India
E-mail: dchopra@iiserb.ac.in

MS received 21 February 2019; revised 9 August 2019; accepted 25 September 2019

Abstract. In this study, we have performed a detailed quantitative analysis of the different intermolecular interactions present in 8-(4-ethoxyphenyl)-1,3-dimethyl-3,7-dihydro-1H-purine-2,6-dione (**I**). The molecule crystallizes in the *P*-1 space group with one molecule in the asymmetric unit. The molecule had a layered crystal packing wherein the molecular sheets are primarily formed by hydrogen bonds and the stabilization is dominated *via* the electrostatic energy contribution. This molecular sheet is then interconnected to other similar sheets *via* different stacking motifs with significant contribution from dispersion energy components.

Keywords. Xanthine derivatives; intermolecular interactions; energy framework analysis; fingerprint plot; electrostatic potential.

1. Introduction

Intermolecular interactions plays a very important role in the determination of the three dimensional arrangement of the molecule in the solid state.[1] Intermolecular interactions present in a molecule are in turn dependent on the nature and strength of the electron donor and electron acceptor groups present in the molecule.[2] It is now well-established that relatively weak intermolecular interactions such as C-H···X(X = halogens/O/S/N, etc.)[3] hydrogen bonds play a crucial role in the crystal packing of different molecules, both in the presence and absence of strong hydrogen bonds such as N/O-H···O/N[4] interactions. Apart from the presence of hydrogen bonds, depending on the molecular structure, the stacking interactions[5] can also play an important role in the crystal packing of molecules.

Xanthine derivatives are a very important class of adenosine receptor antagonists.[6] It is observed, however, that by incorporating different substituents at the 8-position of the purine ring, high selectivity can be achieved for certain subtypes of adenosine receptor.[6,7] However, the synthesis of these compounds is not straight forward and hence several procedures have been developed which are directed towards improving the synthetic yields.[6,7] Given the importance of these compounds in medicinal chemistry,[6b] in the past decade, a detailed investigation on intermolecular interactions present in these molecules in solids is of relevance with special emphasis in the context of crystal engineering.[8] Hence, in this study, we have performed a detailed quantitative investigation of the role of different intermolecular interactions present in the crystal structure of a 8-substituted Xanthine derivative namely 8-(4-ethoxyphenyl)-1,3-dimethyl-3,7-dihydro-1H-purine-2,6-dione (**I**) (Scheme 1) which involves calculations of the interaction energies,[9a] energy framework analysis,[9b] electrostatic potential maps[9c] and 2D finger plot analysis.[9d] using CrystalExplorer17.[10]

2. Experimental

2.1 *Synthesis and characterization*

The compound **I** was synthesized and characterized by following the standard procedure already reported in the literature.[11]

*For correspondence

Published online: 04 January 2020

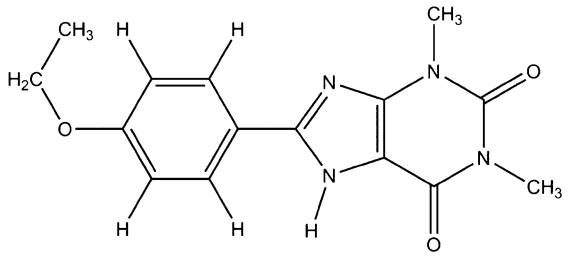

8-(4-ethoxyphenyl)-1,3-dimethyl-3,7-dihydro-1*H*-purine-2,6-dione

Scheme 1. Molecular structure of I investigated in this study.

2.2 *Crystallization*

Good quality single crystals of I was obtained *via* solvent evaporation method using 1:1 mixture of DMSO:methanol at room temperature (25 °C).

2.3 *Single crystal X-ray diffraction*

Single crystal X-ray diffraction data of **I** were collected on a Bruker APEX-II diffractometer equipped with a CCD area detector using Mo Kα radiation (λ = 0.70173 Å) in φ and ω scan modes at 100(2) K. Cell refinement and data reduction were performed using the program SAINT (Bruker AXS). The data were scaled and absorption correction was performed using SADABS (Bruker AXS). The crystal structure was solved by direct methods using SIR 92[12] and refined by the method of least-squares on the basis of all observed reflections using SHELXL-2014[13] present in WinGX (version 2014.1).[14] Non-hydrogen atoms were refined with anisotropic displacement parameters. The molecular connectivity and the crystal packing diagrams were generated using Mercury 3.9 (CCDC) program.[15] Geometrical calculations were done using PARST[16] and PLATON.[17] The details of the data collection and structure refinements are shown in Table 1.

2.4 *Theoretical calculations*

All the theoretical calculations in this study was performed using CrystalExplorer17.[10] All the hydrogens were moved to the neutron positions. Intermolecular interaction energies, which were partitioned into Electrostatic (E_{elec}), Polarization (E_{pol}), Dispersion (E_{disp}) and Repulsion (E_{rep}) energy components was calculated at B3LYP/6-31G** level of theory. The obtained interaction energies were further utilized to map the network of energy frameworks across different planes. The concept of energy frameworks allows for a better understanding of the intermolecular interactions as it graphically represent the total interaction energies or its individual components as cylindrical tubes joining the molecules.[9b] The radii of these cylinders is directly proportional to the strength of the corresponding intermolecular interactions. The Molecular Electrostatic Potential Map (MESP) was plotted on the Hirshfeld isosurface at B3LYP/631G** level. The contribution of different intermolecular interaction was also further quantified *via* 2D Fingerprint plot.

Table 1. Crystallographic and Refinement Data

Code	**I**
CCDC No.	1888205
Formula	$C_{15}H_{16}N_4O_3$
Formula Weight	300.32
Crystal System	Triclinic
Space Group, Z	*P*-1, 2
a (Å), *b* (Å), *c* (Å)	5.0565(9), 11.746(2), 12.223(3)
α (°), β (°), γ (°)	91.112(8), 100.597(7), 94.361(7)
Temperature (K)	100(2)
Volume (Å^3)	711.1(2)
Wavelength (λ)	0.71073
Density (g cm^{-3})	1.398
No. of reflections collected	7599
No. of unique reflections	2842
$2\theta_{max}$ (°)	26.37
No. of parameters	263
R_1, wR_2 ($I > 2\sigma$)	0.0531, 0.1156
G.o.F	0.986

3. Results and Discussion

3.1 *Molecular structure and electrostatic potential map*

The compound **I** crystallizes in *P*-1 with one molecule in the asymmetric unit. The *ORTEP* of the molecule is shown in Figure 1. The analysis of the electrostatic potential map of **I** (Figure 2) reveals that the most electrostatic negative region belongs to the carbonyl oxygens (O1, O2), present in the molecule with the magnitude being in range of −150 to −225 kJ/mol. In comparison, the magnitude of the negative electrostatic potential on the oxygen of the ethoxy group (O3) was calculated to be in the range of −25 to −90 kJ/mol, of considerably reduced magnitude. The difference in the magnitude of the negative electrostatic potential around the different oxygen atoms clearly shows the effect of the electronic environment on the electrostatic potential distribution of a given atom. One of the nitrogens of the purine ring (N4) also has a significant magnitude of the negative electrostatic potential (−55 to −90 kJ/mol). While the remaining nitrogens (N1, N2, N3) also have a negative electrostatic potential, the magnitudes were significantly

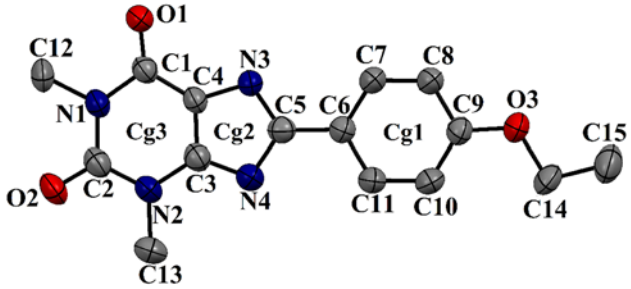

Figure 1. *ORTEP* of I drawn at 50% ellipsoidal probability along with the numbering scheme. Hydrogen atoms were removed. Cg1: ring formed by C6-C11, Cg2: ring formed by C3-C4-N3-C5-N4, Cg3: ring formed by C1-N1-C2-N2-C3-C4.

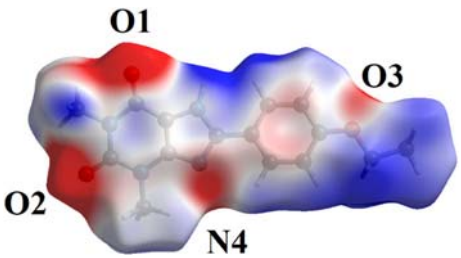

Figure 2. Electrostatic Potential Map of **I** drawn on Hirshfeld isosurface. The scale of the electrostatic potential ranges from − 18 kJ/mol (red) to +18 kJ/mol (blue).

lower than the other nitrogen or oxygen atoms due to changes in the electronic environment around these atoms (Figure 2). The region above the Cg1 ring exhibits negative electrostatic potential while the purine ring (Cg2 and Cg3) had regions of positive electrostatic potential above the π-region. The most positive electrostatic potential region belongs to the presence of the highly acidic N-H hydrogen, with a magnitude of ∼564 kJ/mol. In comparison, the magnitude for the hydrogens attached to sp^2 carbon and to sp^3 hybridized carbon were approximately in the range of 40 to 150 kJ/mol.

3.2 *Crystal packing and energy framework analysis*

The intermolecular interactions present in the crystal structure of **I** are reported in Table 2 along with the respective interaction energies. The most stabilized molecular pair in **I** (motif **i**, Figure 3a) consists of a short and directional N-H···O interaction ($d_{H\cdots O}$ = 1.75Å, ∠N-H···O = 178°). This motif is further supported by presence of a C-H···O interaction ($d_{H\cdots O}$ = 2.32Å, ∠C-H···O = 158°) resulting in the overall stabilization energy of −94.0 kJ/mol (Table 2) with 88% contribution from the electrostatic (coulombic + polarization) component towards stabilization. Along the *c*-axis, motif **i** is connected to another similar motif *via* motif **vi** (Figure 3f) resulting in the formation of ···ABABAB··· type molecule chain (Figure 4a). Motif **vi** (−16.1 kJ/mol) consists of weak H···H contacts (Table 2) which are highly dispersive in nature with 85% contribution towards stabilization. Similar molecular chains are then interlinked to each other by the utilization of motif **vii** (−14.1 kJ/mol, Figure 3g) and **viii** (−11.4 kJ/mol, Figure 3h) down the *bc*-plane, thus giving rise to the presence of a planar molecular sheet (Figure 4a). Motif **vii** is stabilized by the presence of two unique C-H···O interactions (Figure 3) and motif **viii** is primarily stabilized by weak and

Table 2. Intermolecular interactions along with geometrical parameters and respective interaction energies portioned into different energy components.

Motif	Symmetry Operation	Interactions	d (Å)/∠(°)	E_{coul} (kJ/mol)	E_{pol} (kJ/mol)	E_{disp} (kJ/mol)	E_{rep} (kJ/mol)	E_{total} (kJ/mol)
i	2-x, 1-y, 1-z	N3-H1···O1	1.75/178	−125.4	−21.5	−26.6	79.5	−94.0
		C7-H7···O1	2.32/158					
ii	− 1+x, y, z	C12-H12A···N2	260/158	−14.9	−2.4	−66.6	23.9	−60.1
		C13-H13C···O2	2.62/147					
		C1(Cg3)···C5(Cg2)	3.451(2)					
		C14-H14B···Cg1	2.71/143					
iii	1-x, 1-y, 1-z	C14-H14A···N4	2.89/169	−7.5	−1.2	−30.7	8.8	−30.6
		Molecular Stacking	–					
iv	1-x, 1-y, 1-z	Molecular Stacking	–	2.3	−1.6	−29.6	7.4	−21.2
v	2-x, 2-y, 1-z	C12-H12B···O2	2.78/123	−3.8	−1.8	−17.3	6.3	−16.7
vi	-x, 1-y, 1-z	C10-H10···H10	2.03/149	−2.3	−1.5	−22.3	10.1	−16.1
		C11-H11···H14B	3.02/133					
vii	-1+x, -1+y, z	C8-H8···O2	2.68/170	−6.5	−1.2	−10.2	3.8	−14.1
		C13-H13B···O3	2.86/127.8					
viii	3-x, 2-y, 1-z	N-(CH_3) ··· (CH_3)-N	–	−5.9	−1.9	−12.8	9.2	−11.4

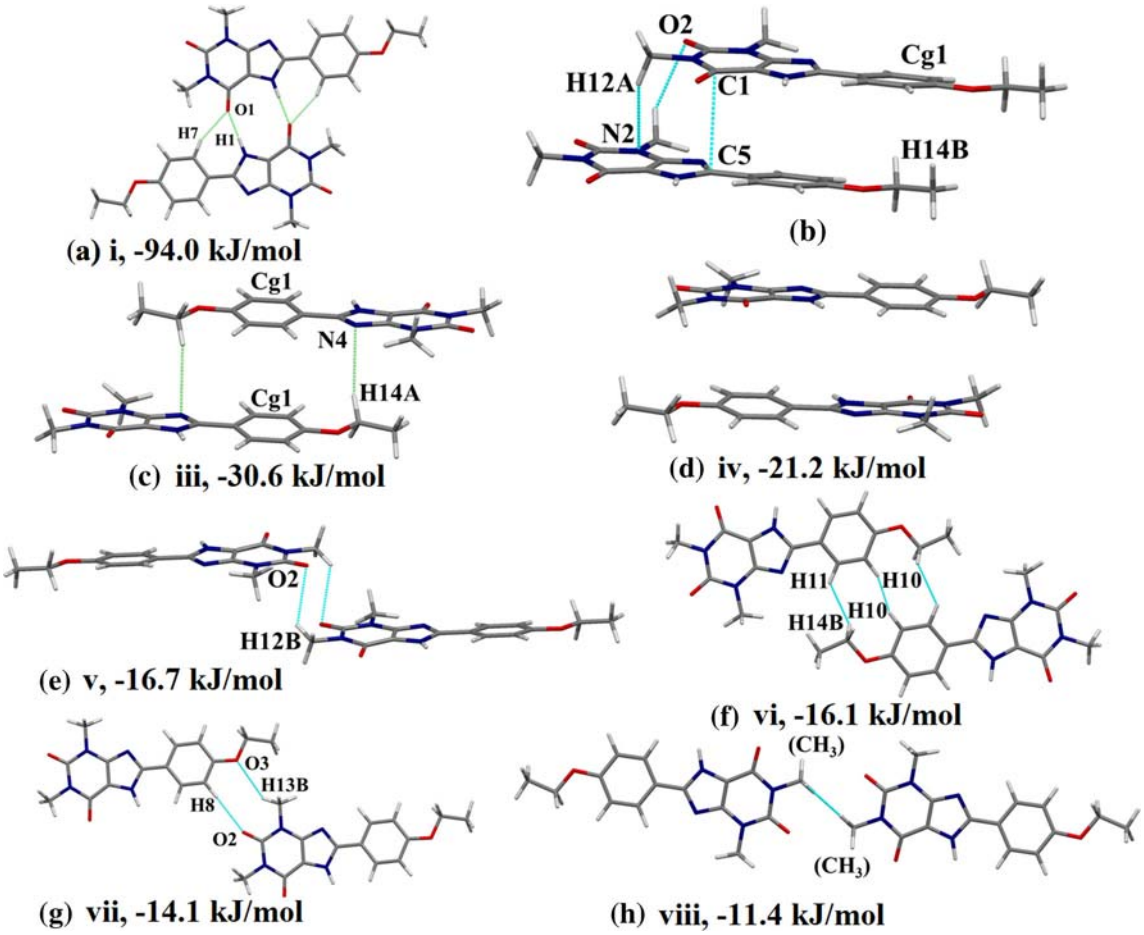

Figure 3. Different molecular pairs **i–viii** extracted from the crystal packing of **I** along with the total interaction energies.

dispersive (60% contribution towards stabilization) N-(CH_3)···(CH_3)-N contacts. The energy framework (Figure 4b–d) down this molecular sheet is clearly dominated by the electrostatic component (Figure 4b), ∼70% (−166.2 kJ/mol, from motif **i+vi+vii+viii**) towards stabilization as compared to the significantly lower contribution from the dispersion component (Figure 4c) with ∼30% (−71.9 kJ/mol, from motif **i+vi+vii+viii**) towards stabilization. This is also the reason why the energy framework representing the total energy (Figure 4d) closely resembles the energy framework drawn with the contribution of the electrostatic energy only (Figure 4b).

The molecular sheets (formed by motif **i**, **vi–viii**) are then connected to other similar molecular sheets *via* four highly dispersive molecular pairs (motif **ii–v**, Figure 3b–e) with greater than 75% contribution from dispersion towards stabilization (Table 2). This significantly high contribution of dispersion is due to the presence of molecular stacking (not necessarily π···π interaction) in these four motifs (Figure 3b–e). Motif **ii** consists of C-H···O ($d_{H\cdots O}$ = 2.62Å, ∠C-H···O = 147°) and C-H···N ($d_{H\cdots N}$ = 2.60 Å, ∠C-H···N = 158°) interactions and additionally supported by the presence of C-H···π and π···π interaction resulting in a total interaction energy of −60.1 kJ/mol (Table 2). Motif **iii** is stabilized by the presence of a C-H···N interaction ($d_{H\cdots N}$ = 2.89Å, ∠C-H···N = 169°) interaction. However, the molecules involved in motif **iii** were stacked to each other in a highly displaced manner further contributing towards the stabilization of this motif. Motif **iv** also represents a case of highly displaced molecular stacking with the interaction energy being −21.2 kJ/mol (Table 2). It is also interesting to note that the coulombic contribution is destabilizing in this motif (Table 2) and hence it is entirely stabilized by dispersive contribution (Table 2). Motif **viii** consists of a weak and directional C-H···O interaction. The total energy between different molecular sheets is −128.6 kJ/mol (motif **ii+iii+iv+v**) with contribution of dispersion towards stabilization being ∼82% (−144.2 kJ/mol) as compared to that of electrostatic contribution ∼18% (−30.9 kJ/mol). Hence, here the energy framework

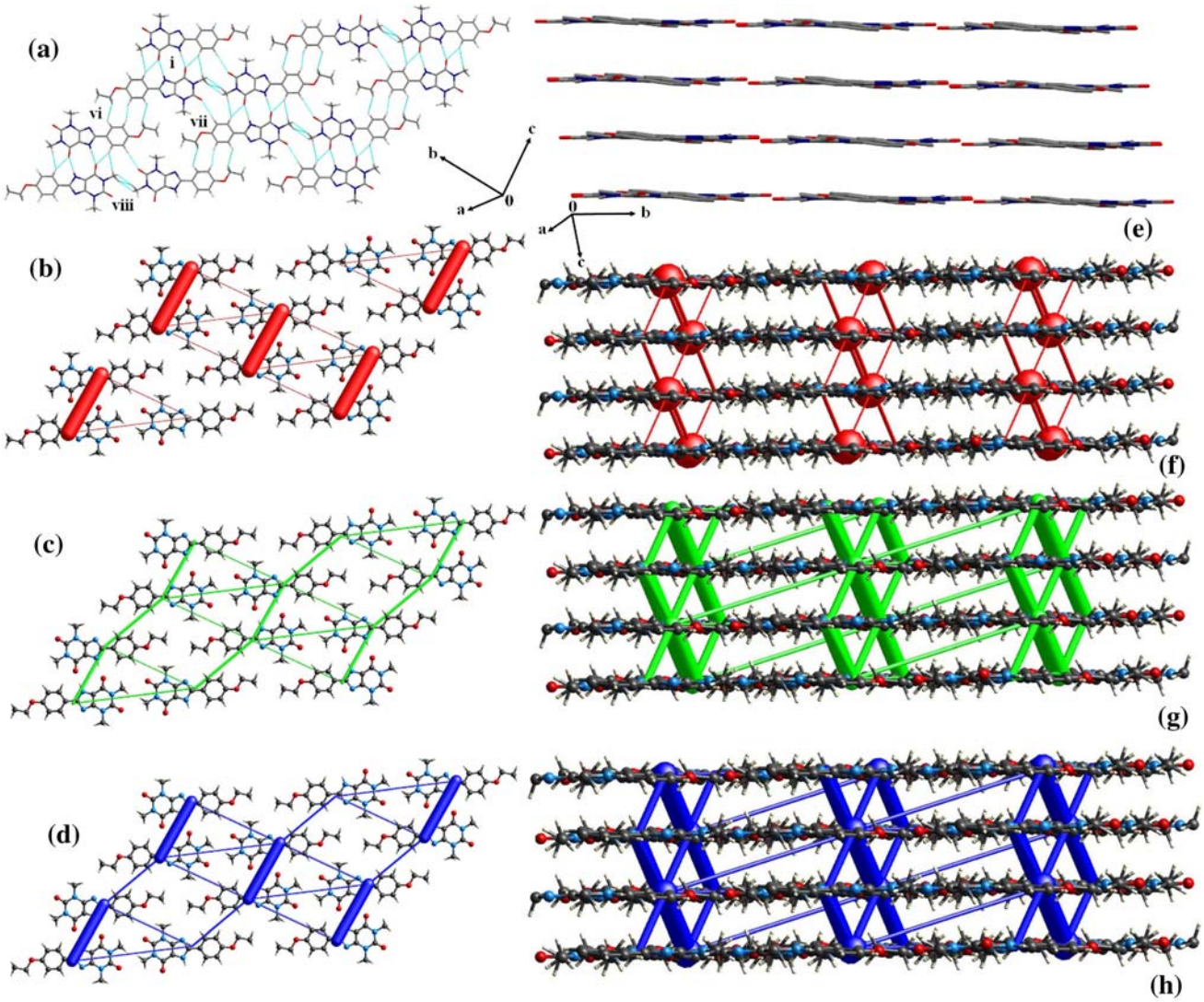

Figure 4. (a) Molecular sheet formed present in crystal packing of **I** and the corresponding energy framework with (b) electrostatic (c) dispersion (d) total energies, respectively. (e) Stacking of different molecular sheets in **I** and the corresponding energy framework with (f) electrostatic (g) dispersion (h) total energies, respectively.

representing the total energy (Figure 4h) is in resemblance with the energy framework representing dispersion component (Figure 4g) as compared to that of the electrostatic energy component (Figure 4f).

3.3 *Hirshfeld fingerprint analysis*

The fingerprint analysis (Figure 5) reveals that the interactions involving hydrogen were the major contributor towards the overall packing with 90% (Figure 5a). As observed in almost all organic molecules, H···H contact was the major contributor with 48% contribution (Figure 5c). Presence of N-H···O and multiple C-H···O interaction resulted in 20% contribution for H···O contacts (Figure 5d) while H···N contact contribution was 5% due to presence of C-H···N interaction (Figure 5f). The H···C contact had a significant contribution of 16% (Figure 5e) in the fingerprint plot. In addition to the C-H···C(π) interaction, the high contribution of H···C contact can also be attributed to the presence of four different stacking molecular pairs (Figure 3) which brought H and C several atoms in close proximity. In comparison to the interaction involving hydrogen, the contribution of non-hydrogen contacts were comparatively low with 3%, contribution each for N···C, O···C and C···C contacts, respectively (Figure 5a).

4. Conclusions

In summary, we performed a detailed quantitative analysis on the intermolecular interactions present in the crystal structure of 8-(4-ethoxyphenyl)-1,3-dimethyl-3,7-dihydro-1H-purine-2,6-dione. Apart from the

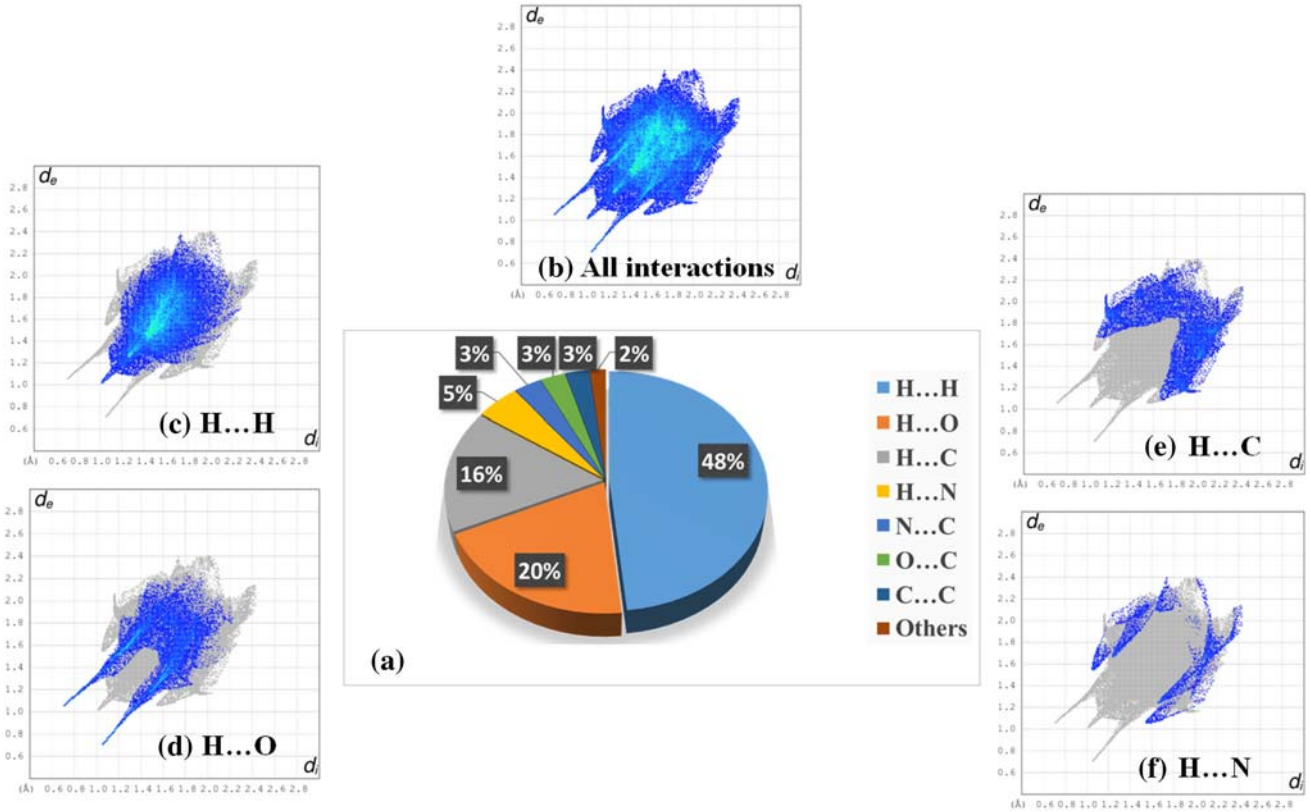

Figure 5. Percentage contribution of different interaction in the crystal packing of **I** along with 2D Fingerprint plot of interactions with significant contribution.

strong N-H···O hydrogen bond, crystal packing of **I** is also stabilized by several relatively weak interactions such as C-H···O, C-H···N hydrogen bonds in addition to H···H contacts and stacking interactions. This study clearly shows that the energetic distribution in the crystal packing is highly anisotropic as is clearly evident from the analysis of the energy frameworks. The molecular sheets present in I which is formed by motif **i**, **vi–viii** had an overall significant contribution from the electrostatic forces as compared to the dispersion. These molecular sheets are then connected to similar sheets *via* highly dispersive intermolecular interactions. This anisotropic distribution of the energetics across different directions is particularly relevant because this feature is generally observed for mechanically flexible crystals.[18] Thus, this study shows that xanthine derivatives may exhibit mechanical response. Hence, it will be of interest in future to analyze the mechanical properties of biologically relevant xanthine derivatives as well.

Acknowledgements

RS thanks DST-INSPIRE for PhD Fellowship. DC thanks IISER Bhopal for infrastructural and research facilities.

References

1. (a) D Chopra (Ed.) 2018 *Understanding Intermolecular Interactions in the Solid State: Approaches and Techniques* (UK: RSC) p. 339; (b) J J Novoa (Ed.) 2018 *Intermolecular Interactions in Crystals: Fundamentals of Crystal Engineering* (UK: RSC) p. 764
2. (a) Bertolasi V, Gilli P and Gilli G 2011 Hydrogen Bonding and Electron Donor−Acceptor (EDA) Interactions Controlling the Crystal Packing of Picric Acid and Its Adducts with Nitrogen Bases. Their Rationalization in Terms of the pKa Equalization and Electron-Pair Saturation Concepts *Cryst. Growth Des.* **11** 2724; (b) Bertolasi V, Gilli P and Gilli G 2012 Adducts of TCNQ with Neutral Nitrogen Bases. Their Rationalization in Terms of Intermolecular Charge-Transfer (CT) or Electron Donor–Acceptor (EDA) Interactions *Cryst. Growth Des.* **12** 4758; (c) Montisci F, Lanza A, Casati N and Macchi P 2018 $NO_2\cdots NO_2$ Contacts under Compression: Testing the Forces in Soft Donor–Acceptor Interactions *Cryst. Growth Des.* **18** 7579
3. (a) Mondal P K, Shukla R, Biswas S and Chopra D 2018 Role of halogen-involved intermolecular inter-actions and existence of isostructurality in the crystal packing of —CF3 and halogen (Cl or Br or I) substituted benzamides *Acta Cryst.* **B74** 574; (b) Shukla R, Nayak S K, Chopra D, Reddy M K and Row T N G 2018 Quantitative investigation of intermolecular interactions in dimorphs of 3-Chloro-N-(2-fluorophenyl)benzamide and 2-Iodo-N-(4- bromophenyl)benzamide *J. Chem. Sci.*

130 38; (c) Nuzzo S, Twamley B, Platts J A and Baker R J 2018 Pseudohalide Tectons within the Coordination Sphere of the Uranyl Ion: Experimental and Theoretical Study of C–H···O, C–H···S, and Chalcogenide Noncovalent Interactions *Inorg. Chem.* **57** 3699; (d) Shukla R, Saeed A, Simpson J and Chopra D 2017 Quantitative investigation of C–H···π and other intermolecular interactions in a series of crystalline N-(substituted phenyl)-2-naphthamide derivatives *CrystEngComm* **19** 5473

4. (a) Dey D and Chopra D 2017 Quantitative analysis of solid-state diversity in trifluoromethylated phenylhydrazones *Acta Cryst.* **B73** 781; (b) Dey D and Chopra D 2017 Occurrence of 3D isostructurality in fluorinated phenyl benzamidines *CrystEngComm* **19** 47
5. (a) Hashim M I, Le H T M, Chen T H, Chen Y S, Daugulis O, Hsu C W, Jacobson A J, Kaveevivitchai W, Liang X, Makarenko T, Miljanic O S, Popovs I, Tran H V, Wang X, Wu C H and Wu J I 2018 Dissecting Porosity in Molecular Crystals: Influence of Geometry, Hydrogen Bonding, and [π···π] Stacking on the Solid-State Packing of Fluorinated Aromatics *J. Am. Chem. Soc.* **140** 6014; (b) Yao Z F, Wang J Y and Pei J 2018 Control of π–π Stacking via Crystal Engineering in Organic Conjugated Small Molecule Crystals *Cryst. Growth Des.* **18** 7
6. (a) Schwabe U, Ukena D and Lohse M J 1985 Xanthine derivatives as antagonists at A1 and A2 adenosine receptors *Naunyn-Schmiedeberg's Arch. Pharmacol.* **330** 212; (b) Singh N, Shreshtha A K, Thakur M S and Patra S 2018 Xanthine scaffold: scope and potential in drug development *Heliyon* **4** e00829
7. Muller C E and Jacobson K A 2011 Recent developments in adenosine receptor ligands and their potential as novel drugs *Biochim. Biophys. Acta* **1808** 1290
8. (a) Desiraju G R 2013 Crystal Engineering: From Molecule to Crystal *J. Am. Chem. Soc.* **135** 9952; (b) Mukherjee A 2015 Building upon Supramolecular Synthons: Some Aspects of Crystal Engineering *Cryst. Growth Des.* **15** 3076
9. (a) Turner M J, Grabowsky S, Jayatilaka D and Spackman M A 2014 Accurate and Efficient Model Energies for Exploring Intermolecular Interactions in Molecular Crystals *J. Phys. Chem. Lett.* **5** 4249; (b) Turner M J, Thomas S P, Shi M W, Jayatilaka M A and Spackman M A 2015 Energy frameworks: insights into interaction anisotropy and the mechanical properties of molecular crystals *Chem. Commun.* **51** 3735; (c) McKinnon J J, Jayatilaka D and Spackman M A 2007 Towards quantitative analysis of intermolecular interactions with Hirshfeld surfaces *Chem. Commun.* 3814; (d) Spackman M A and McKinnon J J 2002 Fingerprinting Intermolecular Interactions in Molecular Crystals *CrystEngComm* **4** 378
10. Turner M J, McKinnon J J, Wolff S K, Grimwood D J, Spackman P R, Jayatilaka D and Spackman M A 2017 CrystalExplorer17 University of Western Australia http://hirshfeldsurface.net
11. Bandyopadhyay P, Agrawal S K, Sathe M, Sharma P and Kaushik M P 2012 A facile and rapid one-step synthesis of 8-substituted xanthine derivatives via tandem ring closure at room temperature *Tetrahedron* **68** 3822
12. Altomare A, Cascarano G, Giacovazzo C and Guagliardi 1993 Completion and refinement of crystal structures with SIR92 *J. Appl. Cryst.* **26** 343
13. Sheldrick G M 2015 Crystal structure refinement with SHELXL *Acta Cryst.* **C71** 3
14. Farrugia L J 2012 WinGX and ORTEP for Windows: an update *J. Appl. Cryst.* **45** 849
15. Macrae C F, Bruno I J, Chisholm J A, Edgington P R, McCabe P, Pidcock E, Monge R L, Taylor R, Streek J V D and Wood P A 2008 Mercury CSD 2.0 - New Features for the Visualization and Investigation of Crystal Structures *J. Appl. Cryst.* **41** 466
16. Nardelli M 1995 PARST95 - an update to PARST: a system of Fortran routines for calculating molecular structure parameters from the results of crystal structure analyses *J. Appl. Cryst.* **28** 659
17. Spek A L 2009 Structure validation in chemical crystallography *Acta Cryst.* **D65** 148
18. (a) Singh M, Bhandary S, Bhowal R and Chopra D 2018 Observation of bending, cracking and jumping phenomena on cooling and heating of Tetrahydrate Berberine Chloride crystals *CrystEngComm* **50** 2253; (b) Bhandary S, Mangalampalli K S R N, Ramamurty U and Chopra D Crystal Structure-Mechanical Property Correlations in N-(3-ethynylphenyl)-3-fluorobenzamide Polymorphs *Cryst. Growth Des.* **18** 47